

## A NEW HALO FINDING METHOD FOR N-BODY SIMULATIONS

JUHAN KIM<sup>1,2</sup> AND CHANGBOM PARK<sup>3,4</sup>

*Not to appear in Nonlearned J., 45.*

### ABSTRACT

We have developed a new halo finding method, Physically Self-Bound (PSB) group finding algorithm, which can efficiently identify halos located even at crowded regions. This method combines two physical criteria such as the tidal radius of a halo and the total energy of each particle to find member particles. No subtle dependence of halo mass functions on various parameters of the PSB method has been found. Two hierarchical meshes are used to increase the speed and the power of halo identification in the parallel computing environments. First, a coarse mesh with cell size equal to the mean particle separation  $l_{\text{mean}}$  is used to obtain the density field over the whole simulation box. Mesh cells having density contrast higher than a local cutoff threshold  $\delta_{\text{LOC}}$  are extracted and linked together for those adjacent to each other. This produces local-cell groups. We analyze the group of particles located at each local-cell group region separately. This treatment makes the halo finding method easily implemented on the parallel computing environments since each computational rank takes the halo identification job in each particle group independently. Second, a finer mesh is used to obtain density field within each local-cell group and to identify halos. We set the cell size of the refined mesh to be twice the gravitational force softening length  $\epsilon$ . The density peaks in the fine mesh are the halo candidates. Based on the fine mesh, we split particles into many groups located in the density shells with different density levels. If a density shell contains only one density peak, its particles are assigned to the density peak. But in the case of a density shell surrounding at least two density peaks, we use both the tidal radii of halo candidates enclosed by the shell and the total energy criterion to find physically bound particles with respect to each halo.

We have tested the PSB using a binary halo model against other popular halo finding methods, such as the Friend-of-Friend (FoF), Spherical Overdensity (SO), DENMAX, and HOP. Similar to DENMAX and HOP, the PSB method can efficiently identify small halos embedded in a large halo, while the FoF and the SO do not resolve such small halos. We apply our new halo finding method to a 1-Giga particle simulation of the  $\Lambda$ CDM model and compare the resulting mass function with those of previous studies. The abundance of physically self-bound halos is larger at the low mass scale and smaller at the high mass scale than proposed by the Jenkins et al. (2001) who used the FoF and SO methods.

*Subject headings:* Cosmology: N-body simulation: halo : halo-finding methods: Numerical

### 1. INTRODUCTION

Cosmological N-body simulations (Park 1990; Gelb & Bertschinger 1994; Park 1997; Evrard et al. 2002; Dubinski et al. 2003; Bode & Ostriker 2003, among others) have been used to test cosmological models in various fields of interests. To compare simulation results with observed galaxies or other visual cosmic objects, one has to extract virialized dark matter halos from the distribution of simulation particles.

An easy way to identify virialized halos from particle distribution is to link particles with distances less than  $l_{\text{FoF}}$  (Friend-of-Friend, Audit et al. 1998; Davis et al. 1985). The value of the linking length  $l_{\text{FoF}}$  is usually set to  $0.2 \times l_{\text{mean}}$  corresponding to the virialization overdensity  $\rho/\rho_b = 178$  (Porciani et al. 2002), where  $\rho_b$  is the mean background density. The chain of linked particles forms a group of particles and the particle group is considered as a virialized halo. But the FoF cannot identify small halos embedded in larger high-density regions.

This effect is similar to the “overmerging” problem occurred in the poor-resolution simulations (Moore et al. 1996; Klypin et al. 1999). The main drawback of the FoF is the “overlinking” (Gelb & Bertschinger 1994) since, in a binary or multiple halo system, member halos are often linked by bridging particles. Then a dumbbell-like halo is identified and, consequently, the halo quantities, such as the center of mass, the shape, the rotation velocity, etc., are blended. The Spherical Overdensity (SO, Lacey & Cole 1994; Warren et al. 1992) uses the mean density for virialized halos. The SO searches for density peaks and puts spheres around them by increasing the radius of the sphere until the internal mean density satisfies the virialization criterion ( $\rho/\rho_b = 178$ ). Particles inside the sphere are grouped as members of the spherical halo. However, small halos embedded in virialized regions can not be properly resolved.

More improved halo finding methods have been proposed in the last decade. The particle sliding scheme in the density field is adopted by the DENMAX (Gelb & Bertschinger 1994) or its variant SKID (Weinberg et al. 1997; Jang-Condell & Hernquist 2001), and the HOP (Eisenstein & Hut 1998). The DENMAX uses rectangular density grid cells to slide particles to the nearby densest grid cell. Then it scoops up particles that are

<sup>1</sup> Korea Astronomy Observatory 61-1, Whaam-Dong, Youseong-Gu, Daejeon, 505-548, Korea

<sup>2</sup> kjhan@kao.re.kr

<sup>3</sup> Korea Institute for Advanced Study 207-43, Cheongnyangni 2-Dong, Dongdaemun-Gu, Seoul, 130-722, Korea

<sup>4</sup> cbp@kias.re.kr

stacked at local density maxima and checks the total energy of each particle to discard unbound particles. The SKID method, an improved version of the DENMAX, uses a variable smoothing length and the density gradient in a coordinate-free density field. The HOP calculates the density field in the way similar to the SKID. However, it uses a different type of particle sliding. The HOP method searches for the maximum density among a particle’s nearest neighbors. Particles are slid into the nearby densest particle. The HOP groups particles in local density maxima as virialized halos similar to the DENMAX.

But above halo finding methods are mainly based only on the density field in determining the member particles of halos. Namely, used are the density-related quantities such as the linking length (FoF), the overdensity (SO), and the sliding on a local density field (DENMAX, SKID, and HOP). As a result, the distribution of particles in a halo depends on the density geometry. For example, the FoF is likely to produce dumbbell-like halos and the SO finds halos with spherical boundaries. Both methods cannot resolve any substructure inside the virialized region. Using the particle sliding scheme seems more proper than the overdensity criteria ( $\rho/\rho_b$  and  $l_{\text{FoF}}$ ) since it is reasonable to assume that boundaries of virialized halos may follow the 3-dimensional density valley when they are next to other halos. But, in some cases, the density gradient field does not properly describe halo boundaries when there is no density valley. For example, consider a small halo is located in a large halo. Around the small halo, there may exist a density valley between the two density peaks of halos. However, there is no density valley in the outskirts of the large halo region beyond the small halo. So the density valley does not form a closed surface. Consequently, particles that are members of the large halo may slide to the small halo along the path without encountering any density valley.

In this paper, we present a new halo finding method based on the density map. However, our method also takes into account the tidal radius that forms a closed surface around the halo and the total energy to select physically bound particles only. We describe how to divide simulation particles into local particle groups in §2. For individual particle groups, we present the way to identify virialized and stable halos in the tidal field in §3. The values of the group finding parameters are given in §4, and we test the sensitivity of the PSB to parameters in §5. In §6, we compare our halo finding method with other popular methods. In §7, we apply our method to the 1-Giga particle simulations. Conclusions follow in §8.

## 2. LOCAL PARTICLE GROUPS ON A COARSE MESH

The PSB is based on the two hierarchical meshes for particle-density field. A low-resolution density field is used to find the “local particle groups”, and for each local particle group we use a high-resolution density field to find density peaks and to divide particles into multiple “particle sets”. The division of whole simulation particles into many local particle groups allows us to reduce computational costs in halo findings.

The PSB uses all simulation particles to build the density field on a coarse mesh with cell size equal to the mean inter-particle separation  $l_{\text{mean}}$ . To assign densities

to the mesh cells we use the  $W_4$  (Monaghan & Lattanzio 1985)

$$W_4(r, h) = \frac{1}{\pi} \begin{cases} (1 - \frac{3}{2}x + \frac{3}{4}x^3) & \text{if } 0 \leq x < 1, \\ \frac{1}{4}(2-x)^3 & \text{if } 1 \leq x < 2, \\ 0 & \text{otherwise,} \end{cases} \quad (1)$$

where  $r$  is the distance of a particle to a grid point,  $h$  is the smoothing length, and  $x \equiv r/h$ . We set  $h$  equal to  $l_{\text{mean}}$  in the coarse mesh. We attach particles to mesh cells as the linked list (Hockney & Eastwood 1981). We extract overdense cells enclosed by an isodensity surface defined by the density contrast threshold  $\delta_{\text{LOC}}$ . These cells are grouped and labeled. To these grouped cells, we attach adjacent underdense mesh cells to avoid sharp boundary truncations of halos. The particles in a local-cell group are found and called the local particle group.

## 3. PARTICLE SET HIERARCHY AND PARTICLE ASSIGNMENT

### 3.1. Local Density Field on a Fine Mesh

For each local particle group, we construct a high resolution density field on a fine mesh with cell size and smoothing length equal to twice the force softening length  $\epsilon$  to resolve small but physically meaningful structures. We search for local density peaks above the density contrast threshold  $\delta_p$ . Those peaks are called halo cores. Around each density peak, we find the minimum density level  $\delta_c$  with which the isodensity surface encloses only that peak (see Fig. 1). Particles in cells surrounded by this isodensity surface are set to be core members of the density peak. We constrain that the number of core particles ( $N_{\text{core}}$ ) should be at least 10 to avoid the detection of spurious peaks induced by the Poisson fluctuation. We assume those core particles as members of the halo. Other remaining particles are divided into subsets located within the density shells having  $N_{\text{level}}$  density levels between  $\delta_{\text{LOC}}$  and  $\delta_{c,\text{max}}$ , the highest  $\delta_c$ . Every density shell encloses at least two halo cores. We call the group of particles in a density shell a particle set (PS). Now we have to assign each of these particles to one of the halo cores.

We illustrate our halo finding method in Figure 1. Shown are two regions surrounded by the outermost density contours with the threshold level  $\delta_{\text{LOC}}$ . As described in the previous section we call each region a local-cell group. The boundaries of the inner-most density region, **P1**, **P2**, and **P3** are found by searching for  $\delta_c$ ’s. Particles in those regions are the core members of each density peak. Now we call each of **P1**, **P2**, and **P3** a halo candidate. To simplify the illustration in Figure 1., we use three density threshold ( $N_{\text{level}} = 3$ ) and get three particle sets spatially split as **A1**, **A2**, and **A3**. But actually, we use  $N_{\text{level}} = 10$ . Particles in the region **A1** may be assigned to one of **P1** and **P2**. Particles in the regions of **A2** and **A3** can be, similarly, assigned to one of the three halos (**P1**, **P2**, and **P3**).

### 3.2. Tidal Radius Criterion

The PSB method uses multiple steps to assign particles to halos. Particle sets are sorted in a decreasing order of density levels. Starting from particles of the top inner-most PS, we apply the total energy check to each particle and the tidal radius criterion to each halo enclosed by the PS. But there needs an iterative scheme in

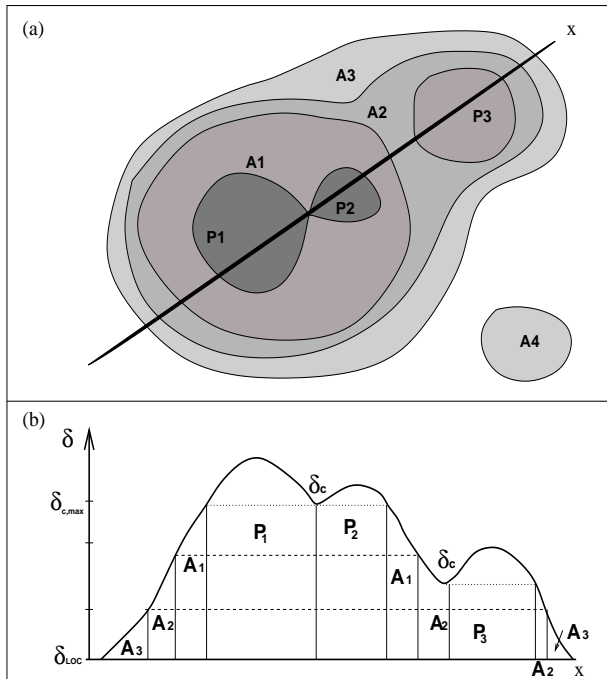


FIG. 1.— Schematic illustration of a density map in our halo finding algorithm. In panel (a), The regions **P1**, **P2**, **P3** and **A4** contain only one density peak with  $\delta \geq \delta_p$ , and are enclosed by isodensity contour surfaces. The regions **A3** and **A4** are identified by the density threshold  $\delta_{\text{LOC}}$ . In panel (b), we show the density map along the line  $x$  in panel (a). A horizontal dotted line shows the core density contrast  $\delta_c$  of each peak. We use  $N_{\text{level}} = 3$  and show the density level in a horizontal dashed line.

this hierarchical membership determination. Since a halo mass is usually measured by its member particles, a halo potential may be underestimated unless all PS's down to the bottom one are taken into account. To supplement the halo mass, we use the PS's having the density levels both higher and lower than that of the current particle set  $\text{PS}_c$ . Let the  $\text{PS}_\downarrow$  be the particle sets geometrically enclosing the halo and having density levels lower than that of the  $\text{PS}_c$ . The potential  $\Phi(k)$  of the  $k$ 'th particle with respect to its host halo is calculated by

$$\Phi(k \in \text{PS}_c) = - \sum_{\ell \in \text{MEM}} \frac{Gm_\ell}{r_{k\ell}} - \sum_{\ell \in \text{PS}_\downarrow} \frac{Gm_\ell}{r_{k\ell}}, \quad (2)$$

where  $r_{k\ell} = |\vec{r}_\ell - \vec{r}_k|$ ,  $m_\ell$  is the  $\ell$ 'th particle mass,  $\text{MEM}$  are the member particles already assigned to the halo in the  $\text{PS}_\uparrow$ 's which have density thresholds higher than that of the  $\text{PS}_c$ . The second term of the right hand side of equation (2) significantly contributes to the particle potential  $\Phi$  if the number of particles in  $\text{PS}_\downarrow$ 's is large. We do not include particles of the  $\text{PS}_c$  for the halo mass in equation (2) since an accidentally close particle to the  $k$ 'th particle can make the potential overestimated.

In some cases, particles happen to be bound to many halos simultaneously. To resolve this situation, we propose a new halo boundary indicator, the tidal radius, which is based on the local gravitational field. A tidal radius of a halo is calculated from a tidal mass  $M_t$  which is the number of only the halo member particles

$$M_t = \sum_{k \in \text{MEM}} m_k. \quad (3)$$

Let  $R_t(i, j)$  be the tidal radius  $R_t(i)$  of the  $i$ 'th halo with respect to the  $j$ 'th halo more massive than the  $i$ 'th. A simple analytic form for the tidal radius is the Jacobi radius  $R_J$

$$R_J(i, j) \equiv D \left( \frac{M_t(i)}{3M_t(j, r < D)} \right)^{1/3}, \quad (4)$$

where  $D$  is the distance between the centers of mass of the halos, and  $M_t(j, r < D)$  is the tidal mass of the  $j$ 'th halo mass contained in a sphere with a radius  $D$ . The effect of underestimation of the halo mass (Eq. 3) on the tidal radius (Eq. 4) is thought to be insignificant due to three reasons. First,  $R_J$  is proportional to its cubic root. Secondly, we measure  $M_t$  at each PS analysis and iteratively update the tidal radius of each halo. Then the tidal radius of a halo converges to a true value when the bottom PS is considered. Thirdly, the  $j$ 'th halo member particles beyond  $D$  do not contribute both to  $M_t(j, r < D)$  and  $M_t(i)$ . The particles of a  $\text{PS}_\downarrow$  that surrounds both the  $i$ 'th and  $j$ 'th halos are usually too far from the two halos to contribute to the tidal masses. And it is less likely for the particles of the  $\text{PS}_\downarrow$  to be assigned to the  $i$ 'th halo and,  $M_t(i)$  is not expected to increase significantly. Therefore, even if we initially assign an inaccurate value to the tidal radius, the tidal radius of each halo converges to a true value in this hierarchical particle assignment process.

However, the Jacobi radius  $R_J$  (Eq. 4) is obtained assuming that  $M_t(i)/M_t(j, r < D) \ll 1$ . To take into account more general situations, we calculate the tidal radius  $R_t$  of a smaller halo as a function of the halo mass ratio  $\mathbf{m} \equiv M_t(i)/M_t(j, r < D)$  using

$$(1 - \tau)^{-2} - \mathbf{m}\tau^{-2} - 1 + (1 + \mathbf{m})\tau = 0, \quad (5)$$

where  $\tau \equiv R_t/D$  (Eq. 7-82 of Binney & Tremaine 1994). We assume that two halos orbit circularly around their center of mass. In Figure 2, we show the ratio of the tidal radius  $R_t$  to the distance  $D$  as a function of the halo mass ratio  $\mathbf{m}$  under various conditions such as the circular orbital motion (Eq. 5, solid curve), the Jacobi limit  $\mathbf{m} \rightarrow 0$  (dotted curve, King 1962; Binney & Tremaine 1994), and no orbital motion (short-dashed curve). As can be seen in Figure 2, our adopted tidal radius model (solid curve) can be approximated by the Jacobi radius  $R_J$  in the limit of  $\mathbf{m} \rightarrow 0$ . However, as  $\mathbf{m} \rightarrow 1$  in a binary system with equal halo masses, the Jacobi radius  $R_J$  approaches an incorrect value of  $0.69D$  while our formula gives  $R_t = D/2$ . We fit our model to a fitting function (Keenan 1981)

$$R_t = D \left[ \frac{M_t(i)}{\alpha(M_t(i) + M_t(j, r < D))} \right]^\beta, \quad (6)$$

where  $\alpha = 4.813$  and  $\beta = 0.318$  (long-dashed curve).

To a small halo many tidal radii can be assigned with respect to other more massive halos enclosed by a given PS. We adopt the minimum value of  $R_t(i)$ 's as

$$R_t(i) = \text{MIN}[R_t(i, j = 1), \dots, R_t(i, j = N_{eh})], \quad (7)$$

where  $N_{eh}$  is the number of enclosed halos with mass satisfying  $M_t(j, r < D_{ij}) > M_t(i)$ , where  $D_{ij}$  is the distance between the  $i$ 'th and  $j$ 'th halos. If a particles is not bound to any halo or beyond the tidal radius of each

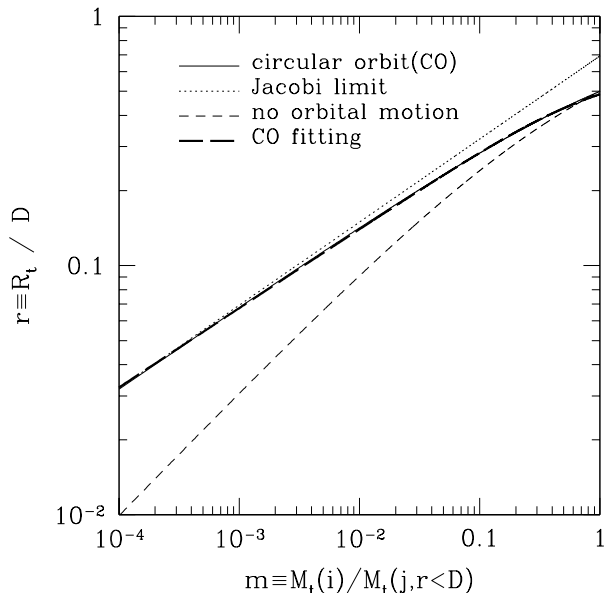


FIG. 2.—  $r$ - $m$  relation. We show the ratio  $r$  of the tidal radius to the distance between halos as a function of the mass ratio between  $M_t(i)$  and  $M_t(j, r < D)$  for the circular orbit (solid curve), for the Jacobi limit (dotted curve, Eq. 4), and for the system with no orbital motion (short-dashed curve). The long-dashed curve shows the fitting result of the tidal radius for a circular orbit system adopted in the PSB method.

halo, we stack it in the free-particle list. Particles in the free-particle list are temporarily added to the particle list of the next PS.

After completing the above steps for all PS's we use the Friend-of-Friend (FoF) method with  $l_{\text{FoF}} = 0.2 \times l_{\text{mean}}$  to find particles belonging to virialized halos. Particles which are not members of any halo are stacked in the free-particle list again.

Before we get final halo data, we check whether or not halos are self-bound and virialized. This process is similar to those of other halo finding methods except for the tidal radius criterion. We find the minimum tidal radius of each halo using equation (7). At this time,  $N_{eh}$  is the number of all halos more massive than a given halo in the local-cell group region. We look into the member-particle and free-particle lists. Unbound particles or those beyond the tidal radius of a halo are discarded and stacked to the free-particle list. We iterate this process four times to obtain self-bound and stable halos. Finally, the FoF method is applied to satisfy the virialization condition of each halo.

The PSB method is summarized in the flowchart in Figure 3. In panel (A), we show the pre-halo finding process described in §2. To find local particle groups, we calculate the density on a low-resolution mesh using all simulation particles. Using densities on the mesh and a pre-defined parameter  $\delta_{\text{LOC}}$ , we find overdense cells and link them making local-cell groups. Particles on the linked cells are grouped and extracted forming local particle groups. Using a local particle group, the PSB method identifies virialized halos. Panel (B) shows a flowchart of the halo finding process on a fine mesh. After finding particle sets, we iteratively update the tidal radius

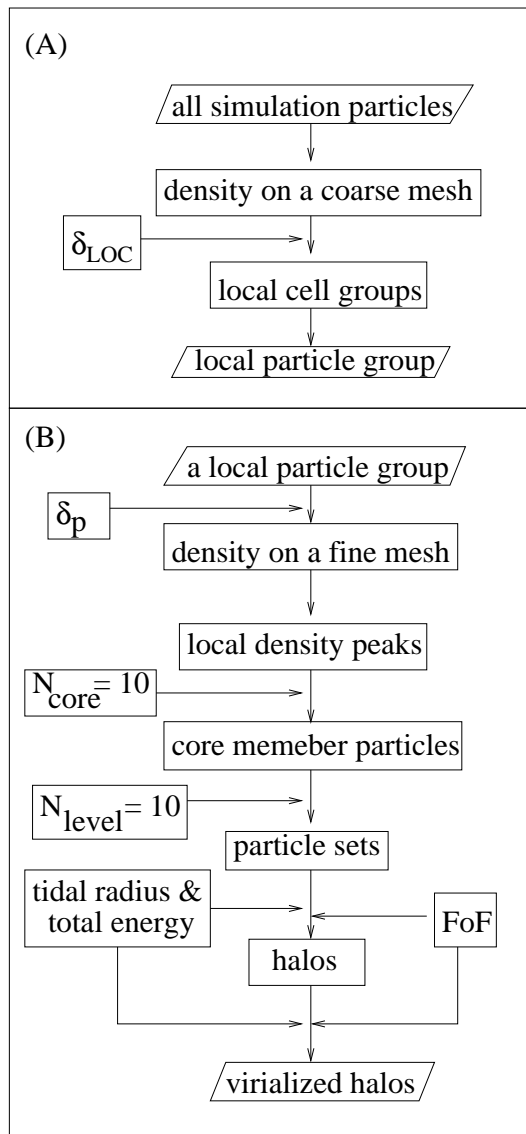


FIG. 3.— Flowchart of the PSB method. We show the way to extract local particle groups based on a coarse mesh described in panel (A), and to identify virialized halos from a local particle group in panel (B). There are four critical parameters used in the PSB method, such as  $\delta_{\text{LOC}}$ ,  $\delta_p$ ,  $N_{\text{core}}$ , and  $N_{\text{level}}$ .

of a halo and calculate the total energy of member particles. We, then, apply the FoF method to find member particles which satisfy the virialization condition.

### 3.3. Parallelization

We parallelize our halo finding method using the Message-Passing-Interface (MPI) library. As described previously, the PSB method is based on two meshes with coarse and fine cells. It therefore adopts two different modes of domain decomposition. Since a coarse mesh is built over the entire simulation box, it is desirable for each computational rank to have the same domain size. We use the domain decomposition into the z-directional domain slabs as described in the GOTPM code (Dubinski et al. 2004). We search for overdense cells and connect them together. Overdense cells at the upper and lower boundaries of local domains can be linked to neighboring

domains. Because we use one-dimensional cyclic ordering of local domains, we pad images of mesh slices imported from neighboring domains at the upper and lower boundaries of the local domain. Those imported mesh slices contain local informations of their domains. We also take account of the periodic boundary conditions of the domain slab in the horizontal directions. With these linked groups of cells, we pick up particles in the overdense cell regions and save those particles to disk.

On the fine mesh the domain decomposition is made based on the local particle group. We set a master rank to do the disk I/O of the local particle data and to distribute them into one of the slave rank that is idle at that time. Each slave rank receives particle data and performs the process described in the §3.1 and §3.2. After finishing the halo finding procedure in a local particle group, the slave rank sends halo member particles back to the master rank to save the halo finding results.

#### 4. PARAMETER DETERMINATION

The lower  $\delta_{\text{LOC}}$  is, the smaller are the smallest halos identified. Two important factors constraining  $\delta_{\text{LOC}}$  are the computer memory available for each rank and the maximum allowable number of density peaks in a local particle group. Since a fine mesh devours much memory budget, the mesh with about  $750^3$  cells is the maximum allowable size on 32bit machines. Second, the tidal radii should be measured for a larger number of density peaks when there are many density peaks in a local particle group. Counting particles to measure  $M_i(j, r < D)$  in eq. (6) with respect to every smaller halo consumes a lot of CPU time.

We have empirically found that it is adequate to set  $\delta_{\text{LOC}} = 1 - 3\sigma_2(0)$ , namely,  $\delta_{\text{LOC}} \sim \sigma_2(0)$  for the case of the SCDM and  $\delta_{\text{LOC}} \sim 3\sigma_2(0)$  for the case of the concordance  $\Lambda$ CDM model where  $\sigma_2(0)$  is the standard deviation of density fluctuation measured in the coarse mesh at  $z = 0$ . We use a constant value of  $\delta_{\text{LOC}}$  at all redshifts. A lower value of  $\delta_{\text{LOC}}$  enable one to identify smaller halos in the lower density regions, but the volume of each local-cell group increases significantly. In the extreme case of  $\delta_{\text{LOC}} = -1$ , there is one big local-cell group containing all simulation particles. Therefore, the advantage of dividing all simulation particles into multiple local particle groups is no more sustained. On the other hand, higher value of  $\delta_{\text{LOC}}$  is not desirable since the tidal radii can be underestimated due to the insufficient description of the local tidal field. Additionally, small halos residing in lower dense regions can be missed in the process of the halo findings. We choose larger  $\delta_{\text{LOC}}$  for the  $\Lambda$ CDM model because the  $\Lambda$ CDM model has higher degree of connectivity of overdense regions (filamentary structures) than the SCDM model. Above values of  $\delta_{\text{LOC}}$  are determined for 2GB memory budget. If more memory budget is available, we are able to reduce  $\delta_{\text{LOC}}$  and identify smaller halos in lower dense regions.

To avoid detecting spurious density peaks, we require density peaks to have at least two particles in the fine mesh cell. The density corresponding to this constraint is

$$\delta \sim 2 \times (l_{\text{mean}}/l_f)^3, \quad (8)$$

where  $l_f$  is the cell size of the fine mesh. If  $l_{\text{mean}}/l_f = 5$ , then  $\delta \sim 250$ . A halo having the density peak cell with

two particle satisfies the virial condition  $\delta_{\text{vir}} \geq 177$  automatically. Two density parameters  $\delta_{\text{LOC}}$  and  $\delta_p$  should satisfy the virial condition,

$$\delta_{\text{LOC}} \ll \delta_{\text{vir}} < \delta_p. \quad (9)$$

In the PSB method, two density meshes with different cell sizes are adopted and different density thresholds,  $\delta_{\text{LOC}}$  and  $\delta_p$ , are applied to them. Occasionally, there may be peaks with  $\delta > \delta_p$  at the scale of the fine cell but with  $\delta < \delta_{\text{LOC}}$  on the coarse cell. We estimate the fraction of such missing peaks in the following to show the problem is minor for our choice of  $\delta_{\text{LOC}}$  and  $\delta_p$ .

For a Gaussian density field, the probability of finding the regions with  $\delta \geq \delta_t$  is

$$P[\delta \geq \delta_t] = \frac{1}{\sqrt{2\pi}\sigma} \int_{\delta_t}^{\infty} d\delta' \exp\left(-\frac{\delta'^2}{2\sigma^2}\right), \quad (10)$$

where  $\sigma^2$  is the variance of the density fluctuation. Let us use the subscript 1 to denote the statistical quantities measured in the fine mesh and the subscript 2 in the coarse mesh. In our halo finding method the smoothing lengths  $h$ 's are set to the mesh cell sizes, namely  $h_1 = l_1 = 2\epsilon$  and  $h_2 = l_2 = l_{\text{mean}}$ . It is usually  $\epsilon = 0.1 \times l_{\text{mean}}$  in high resolution cosmological simulations. The conditional probability that a region has  $\delta \geq \delta_p$  in the fine mesh when it has  $\delta \leq \delta_{\text{LOC}}$  in the coarse mesh is,

$$P[\delta_{h_1} \geq \delta_p | \delta_{h_2} \leq \delta_{\text{LOC}}] = P[\delta_{h_1} \geq \delta_p, \delta_{h_2} \leq \delta_{\text{LOC}}] / P[\delta_{h_2} \leq \delta_{\text{LOC}}]. \quad (11)$$

The joint probability  $P[\delta_{h_1} = \delta_1, \delta_{h_2} = \delta_2]$  is

$$\begin{aligned} & P[\delta_{h_1} = \delta_1, \delta_{h_2} = \delta_2] \\ &= \frac{1}{2\pi\sqrt{|M|}} \exp\left(-\frac{1}{2}\Delta^T M^{-1}\Delta\right) \\ &= \frac{1}{\sqrt{2\pi}\sigma_s} \exp\left[-\frac{1}{2}\left(\delta_1 - \frac{\delta_2\sigma_c^2}{\sigma_2^2}\right)^2 / \sigma_s^2\right] \\ &\times \frac{1}{\sqrt{2\pi}\sigma_2} \exp\left(-\frac{1}{2}\frac{\delta_2^2}{\sigma_2^2}\right), \end{aligned} \quad (12)$$

where

$$\Delta \equiv \begin{pmatrix} \delta_1 \\ \delta_2 \end{pmatrix}, \quad M \equiv \begin{pmatrix} \sigma_1^2 & \sigma_c^2 \\ \sigma_c^2 & \sigma_2^2 \end{pmatrix}, \quad (13)$$

$$\sigma_i^2 = \frac{1}{(2\pi)^3} \int d^3k P(k) |W_{h_i}|^2, \quad (14)$$

$$\sigma_c^2 = \frac{1}{(2\pi)^3} \int d^3k P(k) \tilde{W}_{h_2}^*(k) \tilde{W}_{h_1}(k), \quad (15)$$

$$\sigma_s^2 = \sigma_1^2 - \frac{\sigma_c^4}{\sigma_2^2}, \quad (16)$$

and  $P(k)$  is the power spectrum of the density field. The smoothing kernel  $\tilde{W}_k$  in  $k$ -space is given by

$$\tilde{W}_h(\mathbf{k}) = \frac{1}{(2\pi)^3} \int_0^\infty dr^3 W_4(\mathbf{r}; h) \exp(i\mathbf{k} \cdot \mathbf{r}), \quad (17)$$

and we use a spherically symmetric smoothing window  $W_4$  (Monaghan & Lattanzio 1985). Then, we get

$$\begin{aligned} & P[\delta_{h_1} \geq \delta_p | \delta_{h_2} \leq \delta_{\text{LOC}}] \\ &= \frac{1}{2\pi\sigma_2\sigma_s N} \int_{-1}^{\delta_{\text{LOC}}} d\delta_2 \int_{\delta_p}^{\infty} d\delta_1 \exp\left(-\frac{\delta_2^2}{2\sigma_2^2}\right) \\ &\cdot \exp\left[-\left(\delta_1 - \frac{\sigma_c^2}{\sigma_2^2}\delta_2\right)^2 / 2\sigma_s^2\right], \end{aligned} \quad (18)$$

where

$$N \equiv P[\delta_{h_2} \leq \delta_{\text{LOC}}] = \frac{1}{\sqrt{2\pi}\sigma_2} \int_{-1}^{\delta_{\text{LOC}}} d\delta_2 \exp\left(-\frac{\delta_2^2}{2\sigma_2^2}\right). \quad (19)$$

We have applied our halo finding algorithm to two cosmological N-body simulation data. The simulations are based on a  $\Lambda$ CDM and the SCDM models with the same simulation box size  $L_{\text{box}} = 512h^{-1}\text{Mpc}$ . In the  $\Lambda$ CDM and the SCDM models we follow the gravitational evolution of  $1024^3$  particles in  $1024^3$  mesh cells from  $z = 23$  to  $z = 0$  with 460 time steps by using the GOTPM code (Dubinski et al. 2004). We set  $\delta_{\text{LOC}} = 10$  ( $\simeq 3\sigma_2(0)$ ) for the  $\Lambda$ CDM model and  $\delta_{\text{LOC}} = 5$  ( $\simeq \sigma_2(0)$ ) for the SCDM model, and fix the peak density threshold  $\delta_p = 312.5$ . We calculate the number of unidentified density cells ( $\delta_1 > \delta_p$ ) which reside in the underdense background ( $\delta_2 < \delta_{\text{LOC}}$ ) using equation (18). At  $z = 0$  the number of such density peaks on the fine mesh in the total simulation box is only a few, which is very small compared to the number of halos ( $\sim 2 \times 10^6$  in the  $\Lambda$ CDM simulation and  $\sim 4 \times 10^6$  in the SCDM simulation) identified by the halo finding method.

In some situations, small halos identified in overdense backgrounds may have the true peak densities lower than  $\delta_p$  when the underlying backgrounds are removed. To obtain unbiased halo samples we calculate the halo density by using their member particles at the end of halo identification, and discard the halos having the peak density  $\delta < \delta_p$  from the halo catalog. Finally, for our  $\Lambda$ CDM and SCDM simulation data we obtain halos with masses larger than  $6 \times 10^{11}h^{-1}M_\odot$  ( $\simeq 58$  particles) and  $10^{12}h^{-1}M_\odot$  ( $\simeq 30$  particles), respectively.

### 5. SENSITIVITY TO PARAMETERS

Using halo mass functions, we examine the dependence of halo finding results on the four group finding parameters,  $\delta_{\text{LOC}}, \delta'_p, N_{\text{level}}$ , and  $N_{\text{core}}$ , where  $\delta'_p \equiv \delta_p/125$ . As a testbed, a  $\Lambda$ CDM model is simulated with  $128^3$  particles in a box of size  $128h^{-1}\text{Mpc}$ . The bias factor is set to  $b = 1.11$  and the initial epoch is  $z_i = 4$ . At  $z = 0$ , the RMS of linear density fluctuation on the coarse mesh is 2.69. We use the canonical parameter set  $(\delta_{\text{LOC}}, \delta'_p, N_{\text{level}}, N_{\text{core}}) = (11, 2.5, 10, 10)$ . Then  $\delta'_p \simeq 4.1 \times \sigma_2(0)$ .

In panel (a) of Figure 4, we show halo mass functions with varying  $\delta'_p$  from 1.5 to 2.5. When lower values of  $\delta_p$  are adopted, much more smaller halos are found. In panel (b) the halo mass function shows negligible dependence on  $N_{\text{core}}$ . As the peak parameters,  $\delta_p$  and  $N_{\text{core}}$  are correlated with each other. The variation of  $N_{\text{core}}$  apparently takes no effect on the halo mass functions since  $\delta_p$  is a more stringent parameter when  $\delta_p$  is high enough to satisfy  $\delta_p \geq \delta_{\text{vir}}$ . The dependence of the halo mass function on the threshold density  $\delta_{\text{LOC}}$  is also weak as shown in panel (c). The parameter  $N_{\text{level}}$  hardly affects the halo mass functions as demonstrated in panel (d). We use a high value of  $N_{\text{level}} = 10$  to better resolve clouded regions with many peaks. For example, there are about two thousands peaks in the largest local particle group in our  $1024^3$  particle simulations at  $z = 0$ .

We conclude that the most important parameter is  $\delta_p$  which determines the lower limit of mass of the halos

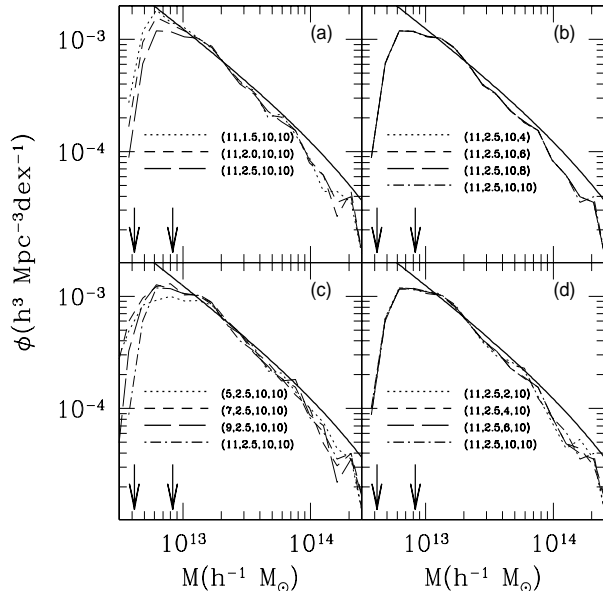


FIG. 4.— Halo mass functions with various different parameter sets. The canonical parameter set is obtained  $(\delta_{\text{LOC}}, \delta'_p, N_{\text{level}}, N_{\text{core}}) = (11, 2.5, 10, 10)$ , where  $\delta'_p \equiv \delta_p/125$ . In panel (a), we show the halo mass functions varying  $\delta'_p$  from 1.5 to 2.5. Panel (b) is same as panel (a), but  $N_{\text{core}}$  is varied. We vary  $\delta_{\text{LOC}}$  in panel (c) and  $N_{\text{level}}$  in panel (d). The solid line shows the Sheth & Tormen mass function, and the two vertical arrows mark the mass of 50 and 100 particles.

found. The role of  $\delta_{\text{LOC}}$  in the PSB method is less significant when  $\delta_p$  is high. But if one wants to identify less massive halos or to reduce  $\delta_p$ , attention must be paid to the value of  $\delta_{\text{LOC}}$ . He must measure the probability of missing fine cells which have  $\delta \geq \delta_p$  in the underdense background ( $\delta \leq \delta_{\text{LOC}}$ ). The other parameters are proved to be insensitive to the halo finding results in the PSB method.

### 6. COMPARISON WITH OTHER HALO FINDING METHODS

We have compared the results of the PSB method with those of other competing halo finding methods. We construct a binary system of halos having 20000 and 1000 member particles, respectively. The large halo has the virial radius  $R = (3M_h/4\pi\bar{\rho}_{178})^{1/3}$ , and the small halo has its tidal radius under the tidal field of the large halo. The distribution of the member particles is set to follow the isothermal density profile. The small halo is slightly offset in x-direction (upper-left panel in Fig. 5). The directions of particle velocities are chosen randomly and the magnitudes are given in accordance with the virialization condition. Here, the small halo is bound to the potential well of the large halo, with no bulk motion. The upper-left panel of Figure 5 shows the particle distribution of each halo with the enlarged particle distribution of the small halo in the inset. We also mark the small halo region with a box in the panel but do not overplot the member particles of the small halo for clarity. The middle-left panel shows the result of the FoF method which does not identify the small halo. The halo boundary found by the FoF method is not smooth due to the Poisson fluctuation of particles at the outskirts of the large halo. The SO method cannot identify the

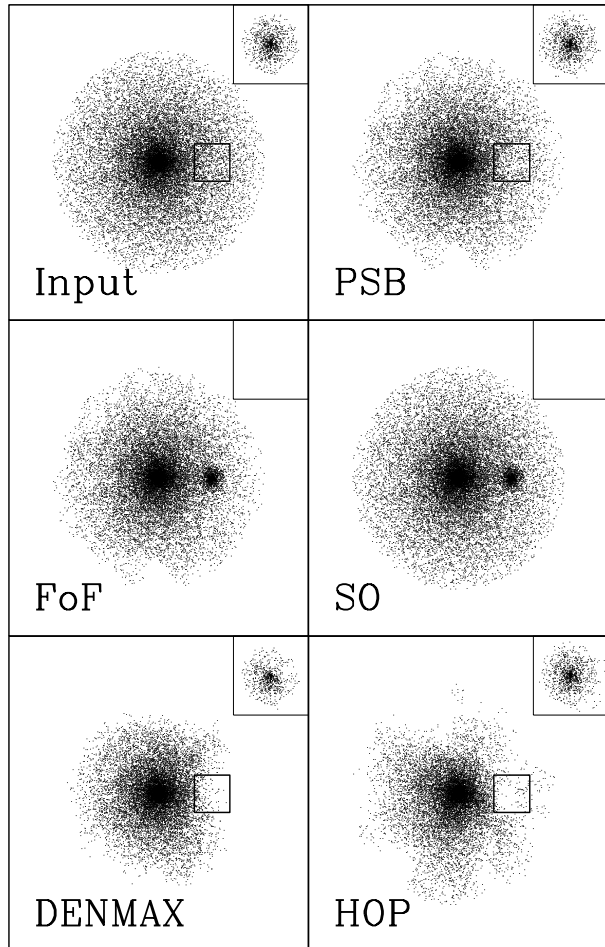


FIG. 5.— Comparison among the results from various halo finding methods. We show the model distribution of particles of two halos in the upper-left panel. The large halo has 20000 particles following the isothermal density profile. The small halo whose region is marked by a box has 1000 particles with the isothermal but tidally truncated density slope. In the inset, we show the enlarged view of the small halo for clarity. The small halo is offset to right with respect to the large halo. We show the identified particle distribution obtained by halo finding methods, such as the FoF (middle-left panel), SO (middle-right panel), DENMAX (lower-left panel), HOP (lower-right panel), and PSB method (upper-right panel). The insets at the upper-right corners show the small halos identified by these methods.

small halo like the FoF method. The large halo is found with a spherical boundary, which is a characteristic of the SO method. These two methods cannot detect the small halo since the halo identification is mainly based on the mean overdensity criterion.

The lower-left panel shows the result of the DENMAX method, which resolves the small halo. However, due to the sliding of particles to the nearby densest cell the large halo seems to have no member particles at the right hand side of the small halo region. All those particles are assigned to the small halo, but they are not bound because of the shallow potential well of the small halo. Consequently, those particles are regarded unbound, and erased from the member list of the small halo. Having the particle sliding algorithm similar to that of the DENMAX, the HOP method can detect particles beyond the

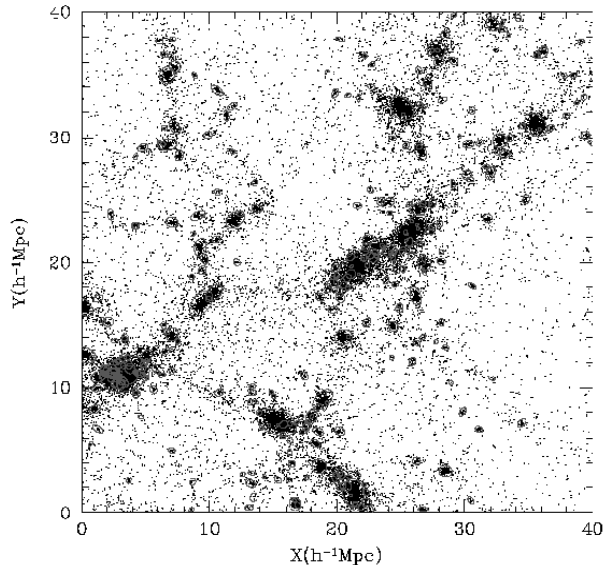


FIG. 6.— Projected particle distribution in the  $\Lambda$ CDM simulation. The thickness of the slice is  $10h^{-1}\text{Mpc}$ . Only every tenth particles in the volume are shown for clarity. Projected ellipsoidal shapes (marked by ellipses) of total 355 halos identified in this volume are shown.

small halo region. Those particles can slide according to local particle links, and possibly make a detouring path around the small halo region to the density maxima of the large halo. Since we do not use the REGROUP algorithm to regroup particles stacked in the local and small density maxima, there are many “particle holes” in the large halo identified by the HOP result.

The upper-right panel shows the result of our PSB method. The boundary of the large halo is similar to that in the FoF method because the FoF method is used in our algorithm to find member particles in the virialized region. The PSB method identifies member particles of the small halo nearly the same as the input. For examples, the numbers of identified member particles of the small halo are 0, 0, 758, 1101, and 1091 for the FoF, SO, DENMAX, HOP, and PSB methods, respectively. Therefore, the PSB method seems to recover the input particle distributions more accurately than other methods except for the HOP. But the density allocation method of the HOP requires more CPU time to search for  $N_{neighbor}$  particles than the PSB method which uses a fixed smoothing length. We conclude that the PSB method is an efficient and accurate halo finding method that can be adapted to the parallel computing environments.

## 7. RESULT OF APPLICATION

### 7.1. Halo Finding for 1-Giga particle simulations

We apply our halo finding method to the 1-Giga particle data simulated on the IBM SP3 at Korea Institute of Science and Technology Information (KISTI) and on a Linux cluster. The times needed to complete the halo findings at  $z = 0$  in the SCDM and the  $\Lambda$ CDM models are about four hours when 32 POWER-4 CPUs are used. In Figure 6, we show the result of halo finding in the  $\Lambda$ CDM model at  $z = 0$ . Only every tenth particles in the volume are shown for clarity. The projected ellip-

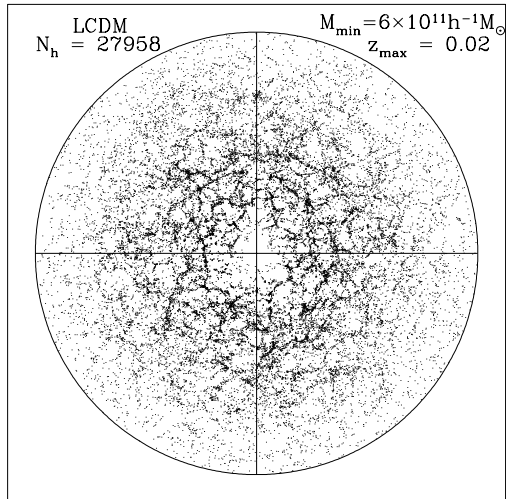


FIG. 7.— A mock redshift survey in the  $\Lambda$ CDM model mimicking the LCRS. The simulated survey slice is  $360^\circ$  by  $4.5^\circ$  wide. Total number of mock galaxies is 27958, with mass  $M \geq 6 \times 10^{11} h^{-1} M_\odot$ . The highest redshift  $z_{max}$  is 0.02.

soidal shapes of halos are plotted on top of the particle distribution.

### 7.2. Mock Galaxy Redshift Survey

Figure 7, shows the distribution of halos in a mock galaxy redshift survey similar to the Las Campanas Redshift Survey (hereafter LCRS, Lin et al. 1996). The selection function adopted here is the same as that of the LCRS. We do not take into account the conversion of halo mass functions to galaxy luminosity functions (Yang et al. 2003). The effects of peculiar velocities of halos are included. The halo number density in our  $\Lambda$ CDM simulation is  $\rho_h = 0.0082 h^3 / \text{Mpc}^3$  which is about 3.5 times less than that ( $\rho_g = 0.029 \pm 0.002 h^3 / \text{Mpc}^3$ ) of the LCRS galaxies in absolute magnitude range  $-23.0 \leq \mathcal{M} - 5 \log h \leq -17.5$ . Using the Schechter function

$$\phi(\mathcal{M}) = (0.4 \ln 10) \phi^* \left[ 10^{0.4(\mathcal{M}^* - \mathcal{M})} \right]^{(1+\alpha)} \times \exp \left[ -10^{0.4(\mathcal{M}^* - \mathcal{M})} \right], \quad (20)$$

where  $\mathcal{M}^* = -20.29$ ,  $\alpha = -0.7$ , and  $\phi^* = 0.019$  (Lin et al. 1996), we find that the mass  $6 \times 10^{11} h^{-1} M_\odot$  corresponds to the magnitude  $-19.8 + 5 \log h$  in the LCRS galaxies from a direct comparison between the cumulative number density of the LCRS galaxies and that of the  $\Lambda$ CDM halos.

### 7.3. Isolated and Distinguished Halos; Halo Mass Function

In this subsection, we compare the halo mass functions found by the PSB and the FoF-like methods with the well-known analytic and fitting functions. We call the halo found by the PSB the distinguished halo. A distinguished halo is a virialized structure irrespective of its environment. For example, each halo in Figure 6 is

regarded as a distinguished halo. The FoF-like halo catalog is constructed by merging halos when halo regions are overlapped. To model each halo as an ellipsoid we use the following shape tensor

$$M_{ij} = \sum_{k=1}^N m_k x_i(k) x_j(k), \quad i, j = 1, 2, 3, \quad (21)$$

where  $m_k$  is the mass of the  $k$ 'th member particle and  $x_i$  is its position with respect to the halo center of mass. The shape tensor  $\mathbf{M}$  is diagonalized for each halo. The ratios of principle axes are the square roots of ratios of the eigenvalues, and the orientations of the axes are the corresponding eigenvectors. However, the volume of the halo cannot be obtained from equation (21). Conserving the ellipsoidal shape of the halo, we scale up and down the shape to include almost all member particles. During the scaling, we set the virial volume to include 95% of member particles since the halo boundary is not smooth. We check whether or not the virial region of a halo overlaps with those of other halos. If overlapping with each other, those halos are merged into a single halo. This merging process is similar to the linking of the FoF method. A halo found by this FoF-like method is a spatially isolated system whose virial region is not shared with other halos. We call this halo an isolated halo.

In Figure 8, we show the halo mass functions of the  $\Lambda$ CDM model simulation at  $z = 0$  measured from the distinguished halo (open circles) and the isolated halo catalogs (crosses). Also shown are other analytic and fitting functions, such as the Press & Schechter (1974, solid curve), Sheth & Tormen (1999, dotted curve), Lee & Shandarin (1998, short-dashed curve), and Jenkins et al. (2001, long-dashed curve) mass functions. In the mass range of  $M_h \leq 2 \times 10^{14} h^{-1} M_\odot$ , the FoF-like method underestimates the number of halos, and overestimates the number of halos with mass  $M_h > 2 \times 10^{14} h^{-1} M_\odot$  when compared with the PSB catalog. Small distinguished halos embedded in dense regions are merged into large halos and, as a result, the mass function of isolated halos approximately follows the predicted mass function of Jenkins et al. (2001) who used the FoF method to find isolated halos in the Hubble Volume Simulations (Colberg et al. 2000). We will study the this isolated and distinguished halos in the forthcoming paper in more details.

## 8. CONCLUSIONS

We provide a new halo finding algorithm that efficiently and accurately identifies halos located in dense environments. This method employs a tidal radius constraint as well as the total energy criterion in determining the halo membership. Based on the density field on a fine mesh with cell size of  $l_1 = 2\epsilon$ , we detect halos with core size down to the force resolution  $\epsilon$ . We have compared the PSB method with other popular halo finding methods in resolving small halos embedded in a larger halo. The FoF and SO methods fail to identify the small halos. The tidal radius of a halo is a physically meaningful boundary descriptor, particularly in crowded regions. Density-related descriptors are not enough to identify halos when they are overlapping each other. When two halos are close to each other, the halos found by the



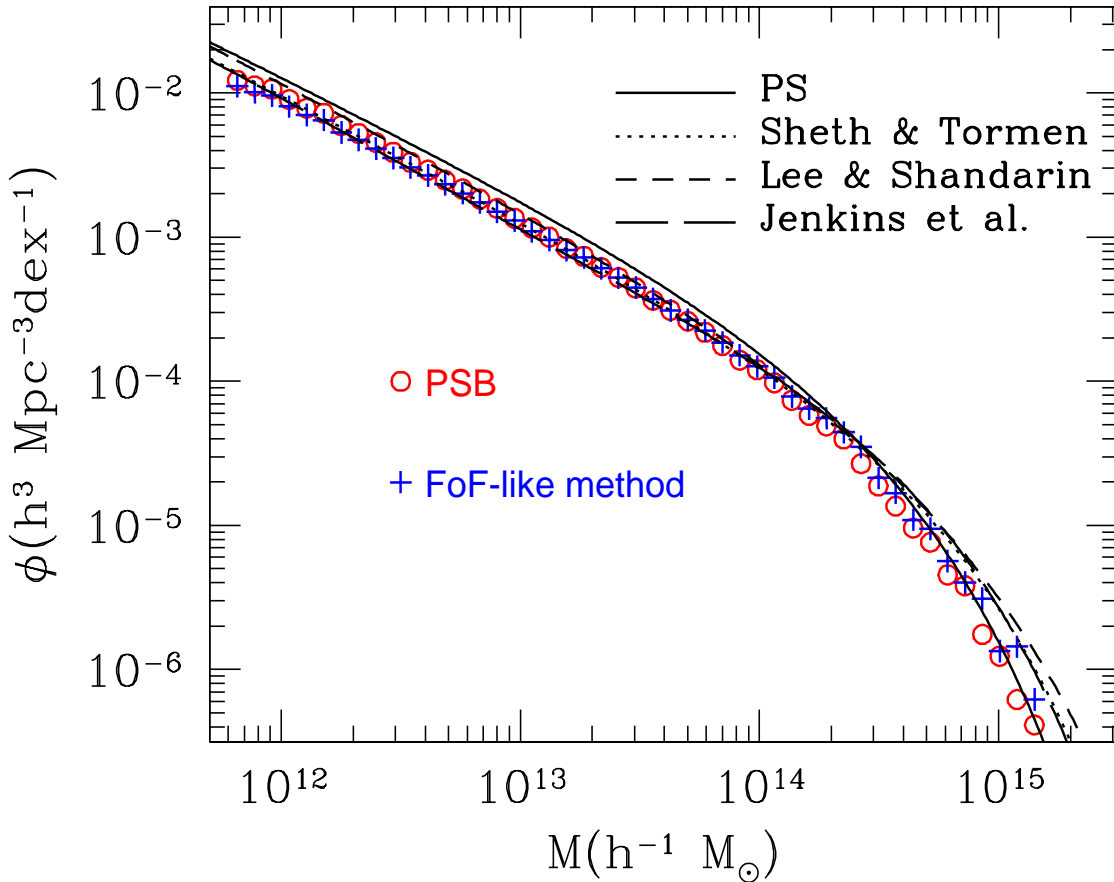


FIG. 8.— Halo mass functions obtained from the  $\Lambda$ CDM model simulation at  $z = 0$ . The halo mass functions obtained by the PSB (open circles) and the FoF-like method (crosses) are shown. We also plot the analytic and fitting functions proposed by Press & Schechter (solid curve), and Sheth & Tormen (dotted curve), Lee & Shandarin (short-dashed curve), and Jenkins et al. (long-dashed curve).

HOP and DENMAX methods may have wrong physical characteristics such as the total mass, shape, spin, peculiar velocity and etc. The adaptive smoothing of the HOP method is not consistent with N-body simulations since the gravitational smoothing length  $\epsilon$  is kept constant throughout whole simulation. It is more reasonable to have the smoothing length  $h$  of the interpolating kernel  $W_4$  equal to  $\epsilon$ . The PSB algorithm is faster than the HOP because of the static smoothing length in obtaining the density field.

The PSB method has several parameters. The most important ones are  $\delta_{\text{LOC}}$  and  $\delta_p$ . We use the constraint of  $\delta_{\text{LOC}} \ll \delta_{\text{vir}} < \delta_p$  to find virialized halos with peak density greater than  $\delta_p$  and to accurately calculate the tidal effect in the local overdense regions ( $\delta > \delta_{\text{LOC}}$ ). With the parameter choices of  $(\delta_p, \delta_{\text{LOC}}) = (312.5, 3-5\sigma_2(0)), (312.5, \sigma_2(0))$  for the concordance  $\Lambda$ CDM and SCDM models, we can identify halos with more than 30 and 58 member particles in each model, respectively. We use the constraint of  $N_{\text{core}} = 10$  to avoid picking up accidentally clustered unphysical peaks. There is another parameter  $N_{\text{level}}$ , the number of density levels which split particles of a local group into at least  $N_{\text{level}}$  particle sets. It is desirable for each particle set to be as small as possible to reduce underestimation of the halo potential

(see Eq. 2). We have found that there is no significant difference in the number of halo member particles if  $N_{\text{level}} \geq 4$ . A parameter dependence study shows that the halo mass function obtained by the PSB method depends sensitively only on  $\delta_p$  at the low mass end. Other parameters such as  $\delta_{\text{LOC}}$ ,  $N_{\text{level}}$ , and  $N_{\text{core}}$ , are rather methodological parameters and basically do not affect the halo finding results.

The main drawback of the PSB algorithm is its memory requirement for the fine mesh. We need two fine meshes; one is for the density map and the other is for the linked list of particles. In 32-bit machines, the maximum allowable number of fine cells is about  $750^3$  which need 3.4 GB memory budget. During the halo finding in the 1-Giga particle simulations, we have found that a few local-cell groups require more memory than the 32-bit limitation. In principle, there is no memory limitation problem on 64-bit machines as far as there is enough physical memory allocated to each CPU. The efficiency of the PSB algorithm decreases when the number of halos increases in a local particle group. The increasing number of halos induces the computational overload to measure the tidal radius with respect to all other massive halos. Therefore, the measurement of a tidal radius scales as  $O(N_h^2)$ . We find that about 30% of the CPU

time in the halo finding is spent in this job. Algorithms faster than the current version of the PSB algorithm are desirable for the next largest simulations.

We apply our method to the 1-Giga particle simulations of the  $\Lambda$ CDM and SCDM models. About four hours are taken for the halo finding in the simulations of the  $\Lambda$ CDM and SCDM models at  $z = 0$  on 32 IBM POWER-4 chips. We expect the PSB method easily scalable to  $2048^3$  or even more massive N-body simulations due to its algorithm of dividing whole simulation particles into multiple local particle groups.

We thank Dr. Jounghun Lee for her useful comments. This work was supported by the Astrophysical Research

Center for the Structure and Evolution of the Cosmos (ARCSEC) of the Korean Science and Engineering Foundation (KOSEF) through Science Research Center (SRC) program, and by the Basic Research Program of the KOSEF (grant no. 1999-2-113-001-5). JK is supported in part by the Project 2003-220-00 of Korea Astronomy Observatory. The authors would like to acknowledge the support from KISTI (Korea Institute of Science and Technology Information) under ‘Grand Challenge Support Program’, and thank Dr. Sangmin Lee for the technical support. The use of the computing system of the Supercomputing Center at KISTI is also greatly appreciated.

#### REFERENCES

- Audit, E., Teyssier, R., & Alimi, J. 1998, *A&A*, 333, 779  
 Bardeen, J.M., Bond, J.R., Kaiser, N., Szalay, A.S. 1986, *ApJ*, 304, 15  
 Bode, P., & Ostriker, J.P. 2003, *ApJS*, 145, 1  
 Binney, J., & Tremaine, S. 1994, *Galactic dynamics*, Princeton University Press, Princeton, New Jersey  
 Colberg, J.M., White, S.D.M., Yoshida, N., MacFarland, T.J., Jenkins, A., Frenk, C.S., Pearce, F.R., Evrard, A.E., Couchman, H.M.P., Efstathiou, G., Peacock, J.A., Thomas, P.A., & The Virgo Consortium 2000, *MNRAS*, 319, 209  
 Evrard, et al. 2002, *ApJ*, 573, 7  
 Davis, M., Efstathiou, G., Frenk, C., & White, S.D.M. 1985, *ApJ*, 292, 371  
 Dubinski, J., Kim, J., Park, C., & Humble, R. 2004, *New Astronomy*, 9, 111  
 Eisenstein, D.J., & Hut, P. 1998, *ApJ*, 498, 137  
 Gelb, J., & Bertschinger, E. 1994, *ApJ*, 436, 467  
 Hockney, R.W., & Eastwood, J.W. 1981, *Computer Simulation Using Particles*, McGraw-Hill, New York  
 Jang-Condell, H., & Hernquist, L. 2001, *ApJ*, 548, 68  
 Jenkins, A., Frenk, C.S., White, S.D.M., Colberg, J.M., Cole, S., Evrard, A.E., Couchman, H.M.P., & Yoshida, N. 2001, *MNRAS*, 321, 372  
 Keenan, D. W., 1981, *A&A*, 95, 340  
 King, I.R. 1962, *AJ*, 67, 471  
 Klypin, A.A., Gottlöber, S., Kravtsov, A.V., & Khokhlov, A.M. 1999, *ApJ*, 1999, 512, 530  
 Lacey, C. and Cole, S. 1994, *MNRAS*, 271, 676  
 Lee, J., & Shandarin, S. 1998, *ApJ*, 500, 14  
 Lin, H., Kirshner, R.P., Shectman, S.A. Landy, S.D., Oemler, A. Turker, D.L., Schechter, P.L. 1996, *ApJ*, 464, 60  
 Monaghan, J.J., & Lattanzio, J.C. 1985, *A&A*, 149, 135  
 Moore, B., Katz, N., & Lake, G. 1996, *ApJ*, 457, 455  
 Park, C. 1990, *MNRAS*, 242, 59p  
 Park, C. 1997, *Journal of Korean Astronomical Society*, 30, 191  
 Porciani, C., Dekel, A., Hoffman, Y. 2002, *MNRAS*, 332, 325  
 Press, W. H., & Schechter, P. 1974, *ApJ*, 187, 425  
 Sheth, R.K., & Tormen, G. 1999, *MNRAS*, 308, 119  
 Warren, M.S., Quinn, P.J., & Salmon, J.K. 1992, *ApJ*, 399, 405  
 Weinberg, D. H., Hernquist, L., & Katz, N. 1997, *ApJ*, 477, 8  
 Yang, X., Mo, H.J., Jing, Y.P., van den Bosch, F.C., & Chu, Y. 2003, preprint(astro-ph/0303524)